

Marangoni-flow-induced partial coalescence of a droplet on a liquid/air interface

Kai Sun,¹ Peng Zhang,² Zhizhao Che,¹ and Tianyou Wang^{1,*}

¹State Key Laboratory of Engines, Tianjin University, Tianjin 300072, China

²Department of Mechanical Engineering, The Hong Kong Polytechnic University, Hong Kong 999077, China



(Received 29 July 2017; published 8 February 2018)

The coalescence of a droplet and a liquid/air interface of lower surface tension was numerically studied by using the lattice Boltzmann phase-field method. The experimental phenomenon of droplet ejection observed by Blanchette *et al.* [*Phys. Fluids* **21**, 072107 (2009)] at sufficiently large surface tension differences was successfully reproduced for the first time. Furthermore, the emergence, disappearance, and re-emergence of “partial coalescence” with increasing surface tension difference was observed and explained. The re-emergence of partial coalescence under large surface tension differences is caused by the remarkable lifting motion of the Marangoni flow, which significantly retards the vertical collapse. Two different modes of partial coalescence were identified by the simulation, namely peak injection occurs at lower *Ohnesorge* numbers and bottom pinch-off at higher *Ohnesorge* numbers. By comparing the characteristic timescales of the upward Marangoni flow with that of the downward flow driven by capillary pressure, a criterion for the transition from partial to total coalescence was derived based on scaling analysis and numerically validated.

DOI: [10.1103/PhysRevFluids.3.023602](https://doi.org/10.1103/PhysRevFluids.3.023602)

I. INTRODUCTION

The coalescence of a droplet with a liquid/air interface is of fundamental relevance to a variety of natural and industrial systems including rain/cloud formation [1], coarsening of emulsions [2], spray atomization [3], and microfluidic devices [4,5]. After the initial contact of the droplet and the interface, a considerable amount of surface energy is converted to the flow kinetic energy and thereby causes significant interfacial oscillation. This, however, does not always result in one-off complete droplet merging with the interface; the occurrence of partial coalescence with concomitant secondary droplets may occur. The secondary droplets may repeat the partial coalescence for several times [6], forming a fascinating coalescence cascade with self-similarity.

Although partial coalescence was first observed half a century ago [7], it was inadequately understood until high-speed cameras and advanced computation techniques became available and affordable in recent years. Thoroddsen and Takehara [6] experimentally identified a cascade of partial coalescence, which stops when the secondary droplet becomes sufficiently small and the viscous effect becomes prominent. Chen *et al.* [8] experimentally observed that the partial coalescence for low-viscosity fluids, occurring for a certain range of drop sizes, exhibits the viscous, the inertio-capillary and the gravitational regimes. Blanchette and Bigioni [9] showed both experimentally and numerically that partial coalescence is caused by the capillary wave convergence on the top of the droplet rather than by the previously recognized Rayleigh-Plateau instability [10]. Ray *et al.* [11] computationally revealed that it is the competition between the horizontal and vertical momentum of

*wangtianyou@tju.edu.cn

the droplet that determines the transition between partial and total coalescence. Honey and Kavehpour [12] experimentally observed that smaller secondary drop bounces higher because of the larger driving capillary force. They also developed a theory that includes the capillary and gravitational forces to predict the maximum height of the bouncing droplet. By using liquid mixtures of different viscosities, Gilet *et al.* [13] found that partial coalescence occurs only when both the *Bond* number (Bo) and the *Ohnesorge* number (Oh) are below certain critical values. At low Bo numbers, the critical Oh number was found to be 0.026 ± 0.003 [10]. Blanchette and Bigioni [14] further determined the critical Oh number as a function of the Bo number as well as of the density and viscosity ratios. In consideration of that droplet coalescence on a flat interface can be conceptually treated as the extreme case of the coalescence of two unequal-sized droplets, Zhang *et al.* [15] experimentally identified the critical larger-to-smaller droplet diameter ratio, above which partial coalescence occurs. This ratio can be as small as 1.55 and increases monotonically with the Oh number.

Most of the previous investigations consider the situation in which the droplet and the interface are made of the same liquid, and little attention has been paid to the situation in which the droplet and the interface are made of different liquids. Because the conversion of surface energy to kinetic energy is critical to the coalescence process, the different surface tensions of the droplet and the interface could be highly consequential, as they often emerge as the result of either temperature difference or composition difference. In this regard, Blanchette *et al.* [16] studied both experimentally and numerically the effect of surface tension gradient on the partial coalescence. They found that partial coalescence is greatly facilitated if the surface tension of the interface, denoted by σ_i , is larger than that of the droplet, denoted by σ_d , and that the total coalescence is facilitated if $\sigma_i < \sigma_d$. Furthermore, if $\sigma_i/\sigma_d < 0.42$, a secondary droplet is ejected from the top of the merged drop. However, the interesting phenomenon of droplet ejection, possibly caused by the Marangoni stress, was not computationally reproduced in Blanchett *et al.*'s paper and left behind the underlying physics to be understood. Martin and Blanchette [17] further considered the situation in which the surface tension difference is induced by surfactant. Their simulations, although not reporting the abovementioned droplet ejection phenomenon, show that the coalescence of a surfactant-free droplet (of a higher surface tension) with a surfactant-laden interface (of a lower surface tension) behaves similarly with the abovementioned coalescence of binary liquids in that a moderate Marangoni effect would suppress partial coalescence. Recently, Shim and Stone [18] experimentally discovered the damped coalescence cascade if $(\sigma_i - \sigma_d)$ exceeds a threshold. In the new regime, the rebound of secondary droplets is suppressed by the accelerated air drainage in the gap, which is driven by the Marangoni flow at every pinch-off.

In spite of these noteworthy advances, the effect of surface tension difference on the coalescence process is still insufficiently understood. Particularly, little effort has been devoted to studying the ejection of secondary droplet when the liquid/air interface has a significantly lower surface tension than the droplet.

In the present study, we aim to numerically investigate the coalescence dynamics of a droplet on a liquid/air interface with $\sigma_i < \sigma_d$, with particular interest in the partial coalescence at sufficiently large surface tension differences. In the following text, the numerical method, the results and discussion, and the concluding remarks are presented in Secs. II to IV.

II. NUMERICAL METHOD

A. Problem specifications

When a droplet comes into contact with a liquid interface, droplet coalescence may take place at the contact point for zero or sufficiently small impact velocity of the droplet, or along a circular rim [19] for a large-velocity impact, which causes a non-uniform concave gas film between the droplet and the interface. In both cases, the flow is symmetric with respect to the axis that is through the center of the droplet and normal to the interface. Consequently, the present numerical simulation was performed in an axisymmetric domain, as illustrated in Fig. 1, where the symmetrical axis is on the left and open boundary conditions are specified on the other sides.

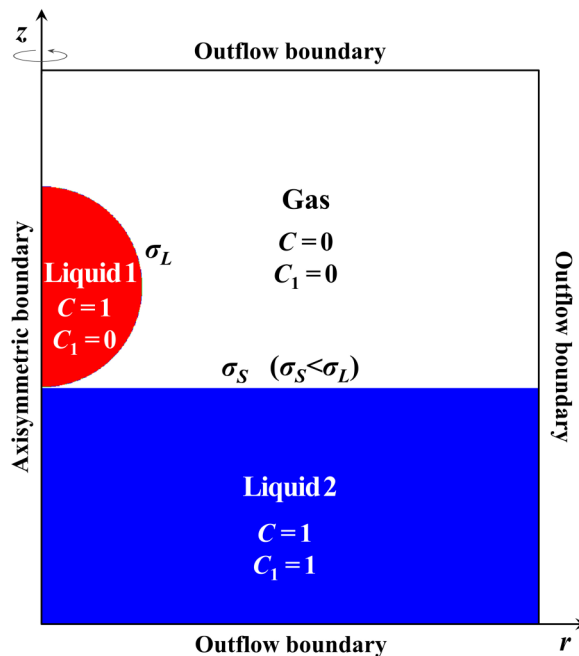


FIG. 1. Specifications of computational domain and boundary conditions.

The reservoir (Liquid 2) and the ambient gas are initially stationary, while the droplet (Liquid 1) is set with a vanishingly small downward velocity to trigger the coalescence. The droplet and the reservoir are assumed to have the same density and viscosity but different surface tensions so that $\sigma_i < \sigma_d$, thereby always inducing a Marangoni flow towards the droplet. For clarity and convenience of the following discussion, we additionally denote $\sigma_i = \sigma_S$ and $\sigma_d = \sigma_L$, where the subscript S and L denote small and large, respectively.

To capture the interfacial flow and the variation in local surface tension, two temporally and spatially varying scalars are employed in the present study. The composition C denotes the volume fraction of liquid either from the droplet or from the reservoir and hence $C = 0$ denotes gas phase and $C = 1$ liquid phase. The composition C_1 stands for the volume fraction of the reservoir fluid and hence $C_1 = 0$ denotes either ambient gas or the Liquid 1 and $C_1 = 1$ the Liquid 2. In short, the droplet, the reservoir, and the ambient gas can be distinguished by $(C = 1, C_1 = 0)$, $(C = 1, C_1 = 1)$, $(C = 0, C_1 = 0)$, respectively. The proportion of Liquid 2 in local liquid is therefore given by $\tilde{C}_1 = C_1/C$.

B. Governing equations with phase-field method

High-fidelity simulation of the present problem could be rather challenging because of the large density jump across the interface as well as the substantial variation in the interfacial stress. In view of the flexibility in handling interfacial flows, the phase-field method, or alternately known as the diffuse-interface method [20,21], is employed in the present study. In this method, the defined composition C is used to capture the interface between the liquid and the ambient gas and is governed by the *Cahn-Hilliard* equation in the form of

$$\frac{\partial C}{\partial t} + \mathbf{u} \cdot \nabla C = M \nabla^2 \mu_C, \quad (1)$$

where \mathbf{u} is the fluid velocity, M the mobility, and $\mu_C = \mu_0 - k \nabla^2 C = \partial E_0 / \partial C - k \nabla^2 C$ the chemical potential with E_0 being the bulk free energy and k the gradient factor. The bulk free

energy can take a double-well function $E_0 = \beta C^2(1 - C)^2$ and the chemical potential is thereby given by $\mu_C = \beta(4C^3 - 6C^2 + 2C) - k\nabla^2 C$ [22].

For single-component two-phase flows, β and k are constants, and the surface tension is determined by $\sigma = \sqrt{2k\beta}/6$. The liquid-gas interface reaches its equilibrium profile as long as the free energy is minimized, and the equilibrium interface profile, $C(z) = 0.5 + 0.5 \tanh(2z/\xi)$, is determined through $\mu_C = \beta(4C^3 - 6C^2 + 2C) - k\nabla^2 C \equiv \text{const}$, in which z is the coordinate normal to the plane interface, and $\xi = \sqrt{8k/\beta}$ is the interface thickness [22]. In the present study, to give rise to the variation in surface tension while maintaining a uniform interface thickness, both β and k are taken as variables with respect to the local surface tension by $k = k_0\sigma/\sigma_L$, and $\beta = \beta_0\sigma/\sigma_L$, where σ/σ_L is determined by \tilde{C}_1 . To avoid the artificial diffusion induced by the mismatch of chemical potential of different liquids, the mobility in Eq. (1) varies as $M = M_0\sigma_L/\sigma$ instead of being a constant. As a result, the relaxation of the liquid/gas interface to its equilibrium state with minimum free energy is completely determined by the composition C .

The composition C_1 is treated as a passive scalar and its transport equation is given by

$$\frac{\partial C_1}{\partial t} + \mathbf{u} \cdot \nabla C_1 = \nabla \cdot (D\nabla C_1) + \tilde{C}_1 M \nabla^2 \mu_C, \quad (2)$$

where D is the composition diffusivity, and the second term on the RHS of Eq. (2) describes the variation of C_1 caused by the *Cahn-Hilliard* diffusion of the liquid/gas interface. It is noted that, since C_1 involves the interface between the gas and Liquid 2, its transport requires minimizing the free energy of the subsystem and thereby maintaining the gas/Liquid 2 interface close to the equilibrium profile, which is realized by the last term in Eq. (2).

In addition to Eqs. (1) and (2), the continuity equation and the momentum equation for incompressible fluids are given by

$$\nabla \cdot \mathbf{u} = 0, \quad (3)$$

and

$$\rho \left[\frac{\partial \mathbf{u}}{\partial t} + \mathbf{u} \cdot \nabla \mathbf{u} \right] = -\nabla p + \nabla \cdot [\mu(\nabla \mathbf{u} + \nabla \mathbf{u}^T)] + \mu_C \nabla C + |\nabla C|^2 \nabla k - (\nabla k \cdot \nabla C) \nabla C, \quad (4)$$

where p is the pressure and μ is the dynamic viscosity. It is noted that the last three terms on the RHS of Eq. (4) represent the interfacial forces: the first one corresponds to the surface tension and the latter two stand for the Marangoni stress. The implementation of the interfacial forces in their potential forms is advantageous to relieve the numerical difficulty in handling interfacial forces. More details on deriving these terms are referred to Refs. [23,24].

C. Numerical implementation

In the present study, Eqs. (1), (3), and (4) are numerically solved in the framework of lattice Boltzmann method (LBM) [25,26]. Two distribution functions are used to capture the liquid/gas interface and to compute the velocity field as well as the dynamic pressure that enforces incompressibility [22,27]. To improve the numerical stability in the simulation of low-viscosity flows, the multiple-relaxation-time collision operator [28] is adopted. It should be noted that, by using the potential form of the interfacial force and the isotropic finite difference, the present numerical methodology is capable of suppressing the well-known spurious current to a relatively low level even at high density ratios [27]. The present numerical methodology has been successfully applied to the simulation of droplet collision/coalescence of both Newtonian and non-Newtonian fluids as well as the dynamics of premixed flames [29–32]. The details about the transformation from the macroscopic governing equations to their corresponding LB equations in an axisymmetric coordinate system have been fully described in the authors' previous paper [29], and they will not be repeated here.

Solving Eq. (2) for the composition C_1 is critical owing to the decisive effect of C_1 on the surface tension distribution. Since the liquid/gas interface occupies only a few grids to minimize its

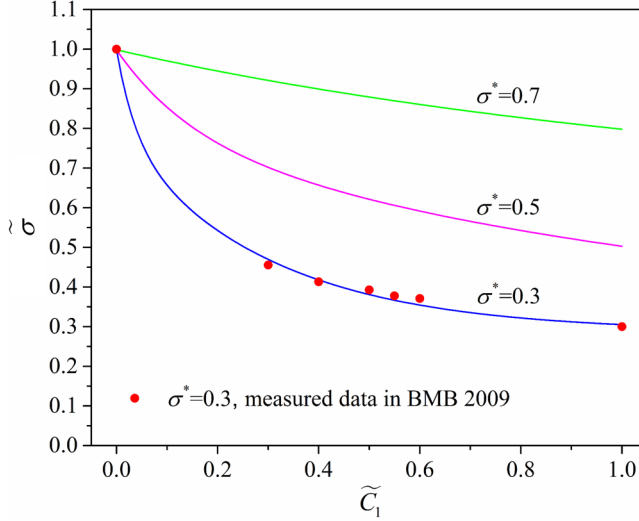


FIG. 2. Dependence of surface tension on the fluid composition. BMB 2009 [16].

finite-thickness effect on the interface dynamics, numerical diffusion of the propagating front of C_1 should be adequately reduced to accurately model the Marangoni flow. Since the accuracy of LBM is only second order in both time and space, the transport equation of composition C_1 , which requires higher accuracy, is solved by using the third-order Runge-Kutta method [33] for time discretization and the fifth-order WENO scheme [34] for spatial discretization.

As for the physical properties, the density is a linear function of C by

$$\rho = \rho_l C + \rho_g(1 - C), \quad (5)$$

where the subscript l and g denote the liquid and the gas phase, respectively. The kinematic viscosity of the fluid is computed by

$$\frac{1}{\nu} = \frac{C}{\nu_l} + \frac{1 - C}{\nu_g}, \quad (6)$$

implying that the collision frequency in the LBM is linearly proportional to C [21].

In the present simulation, the surface tension of the liquid mixture is set according to the experiment of Ref. [16], where the droplet is water and the reservoir is ethanol. The dependence of local surface tension (normalized by $\tilde{\sigma} = \sigma/\sigma_L$) on fluid composition ($\tilde{C}_1 = C_1/C$) is determined by nonlinearly fitting the experimental data, whose apparent nonlinearity shown in Fig. 2 invalidates a linear fitting. It is seen that the fitted curve, $\tilde{\sigma} = \sigma/\sigma_L = f(C_1/C) = f(\tilde{C}_1)$, satisfies the two limiting cases such as $f(\tilde{C}_1 = 0) = 1$ and $f(\tilde{C}_1 = 1) = \sigma_S/\sigma_L = \sigma^* \approx 0.3$ for the water droplet and the ethanol interface. The cases with $\sigma^* < 0.3$ cannot be realized by using these two liquids and therefore are not considered in the present study.

The cases with $\sigma^* > 0.3$ can be obtained by using the mixture of ethanol and water as the Liquid 2 while retaining water as the Liquid 1. The dependence of the variable surface tension on the fluid composition is given by $\tilde{\sigma} = \sigma/\sigma_L = f[\tilde{C}_1 f^{-1}(\sigma^*)]$, where f^{-1} is the inverse function of the fitting function. It is readily seen that the function satisfies the two limiting cases such as $f(\tilde{C}_1 = 0) = 1$ and $f(\tilde{C}_1 = 1) = \sigma^*$.

According to the dimension analysis of the present problem, the six independent non-dimensional parameters to describe flow similarity can be chosen as the normalized surface tension difference $1 - \sigma^*$, the *Ohnesorge* number Oh , the *Weber* number We , the density ratio ρ^* , the viscosity ratio μ^* , and the Schmidt number Sc , as defined in Table I. The Bo number is not necessary since

TABLE I. Nondimensional parameters in the simulation.

Parameter	Value/Range
Normalized surface tension difference $1 - \sigma^* = (\sigma_L - \sigma_S) / \sigma_L$	$0 \sim 0.7$
<i>Ohnesorge</i> number $Oh = \mu_l / \sqrt{\rho_l \sigma_L D_0}$	$0.0018 \sim 0.015$
<i>Weber</i> number $We = \rho_l U^2 D_0 / \sigma_L$	$10^{-4} \sim 1.2$
Density ratio $\rho^* = \rho_l / \rho_g$	500
Viscosity ratio $\mu^* = \mu_l / \mu_g$	50
<i>Schmidt</i> number $Sc = \nu_l / D$	1000

the gravitational force is insignificant compared with the surface tension force in the experiment concerned [16]. In the present simulation, ρ^* and μ^* are fixed at 500 and 50, respectively, and therefore the gas phase does not have significant influence on the droplet coalescence as have been confirmed in many previous studies [14, 16, 19]. The *Sc* number measures the relative importance of momentum transport compared with the composition transport, and it has a typical value of 1000 for binary-liquid system. According to our test, the droplet coalescence process is not significantly affected as long as *Sc* is large (see Supplemental Material [35] for the effect of diffusion on the droplet coalescence process). The *We* number, which is the ratio of the droplet inertia to its surface tension, is set to be 10^{-4} to initiate coalescence without distracting the present focus on the effect of surface tension. It is noted that, a slight overlap between the interfaces, which was used in the authors' previous simulation on the coalescence of two droplets with uniform surface tension [30], is problematic in the present study because it immediately brings out the Marangoni stress and results in the imbalanced stress jump condition cross the local interfaces. This local stress imbalance requires updating the velocity and the pressure fields by solving the governing equations for a few time steps, while the solving process is often subjected to the numerical instability and even causes numerical divergence. In contrast, the present setup of the initial condition is well-posed and numerically stable, and its uncertainty is increasingly negligible by decreasing the initial downward velocity. Using a *We* number as small as 10^{-4} , the possible effects caused by the nonzero droplet initial velocity are minimal.

In the present phase-field simulation, the diffuse liquid/gas interface thickness is resolved by five grids, and the radius (R_0) of the droplet occupies 180 grids to produce grid-independent results (see Supplemental Material [36] for the grid-independence study). The numerical interface *Péclet* number $Pe_i = \xi \sqrt{\sigma_L / (\rho_l R_0)} / (M_0 \beta)$ is fixed at 1.23 to keep the liquid-gas interface close to the equilibrium profile throughout the droplet coalescence processes. The width of the reservoir is set to be $L_r = 5R_0$, which is sufficiently large to eliminate possible boundary effects on the coalescence outcome while keeping an acceptable computational cost (see Supplemental Material [37] for the domain-width-independence study). In the simulation, time is normalized by $t^* = (t - t_0) / t_{osc}$, where t_0 denotes the onset of coalescence, and $t_{osc} = \sqrt{\rho_l R_0^3 / \sigma_L}$ is the characteristic oscillation time of the droplet. A typical run with the present numerical resolution and for a duration of $t^* = 3$ takes about 300 h on an Intel 3.5 GHz Broadwell CPU.

III. RESULTS AND DISCUSSION

A. Experimental verification

Although the experiment on droplet coalescence with an interface of significantly lower surface tension was given by Blanchette *et al.* [16], their simulations were only performed for $(1 - \sigma^*) \leq 0.33$, possibly limited by their numerical method. In the present study, the extreme case of $(1 - \sigma^*) = 0.7$ was successfully simulated to verify the capacity of the adopted methodology. In Blanchette *et al.*'s experiment, the droplet falls down from a syringe and impacts on the reservoir with a nonzero velocity, which is, however, not explicitly given in their paper. By measuring the moving distance

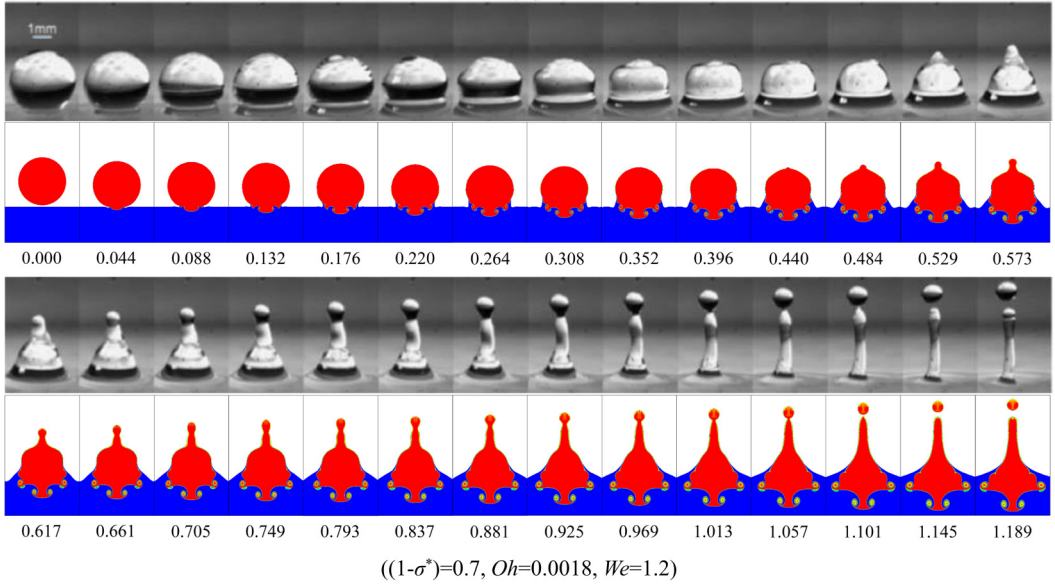


FIG. 3. Experimental verification of droplet ejection at $(1 - \sigma^*) = 0.7$, $Oh = 0.0018$, and $We = 1.2$. The experimental images are adapted from Ref. [16].

of the droplet apex during the first few images in Fig. 2(d) of Ref. [16] and thereby estimating the impact velocity, we found the experimental We number is close to unity.

As shown in Fig. 3, the present method is capable of reproducing the experimental observations, particularly the droplet ejection phenomenon. Two characteristic time instants of the coalescence process, including the emergence of a cusp on the top of the droplet at $t^* = 0.529$ and the pinch-off of a secondary droplet from the liquid column at $t^* = 1.101$, are also well captured.

To quantitatively verify the present simulation in terms of energy conversion among different forms, which poses additional challenges to the numerical methodology with increasing surface tension difference [16], the evolution of various energies during the coalescence was examined and shown in Fig. 4. The total energy (TE) is composed of the surface energy (SE) defined by $SE = \int_s \sigma dS$, the kinetic energy (KE) by $KE = \int_V (\rho u^2/2) dV$, and the cumulative dissipation energy (DE) by $DE = \int_t \Phi dt$, where V , S and t denote volume, surface, and time, respectively. To calculate the surface energy, the liquid-gas interface is chosen as the $C = 0.5$ isosurface. In the axisymmetric coordinates, the viscous dissipation rate Φ is given by

$$\Phi = 2\mu \left[\left(\frac{\partial u_z}{\partial z} \right)^2 + \left(\frac{\partial u_r}{\partial r} \right)^2 + \left(\frac{u_r}{r} \right)^2 \right] + \mu \left(\frac{\partial u_r}{\partial z} + \frac{\partial u_z}{\partial r} \right)^2 - \frac{2}{3} \mu \left[\frac{1}{r} \frac{\partial(ru_r)}{\partial r} + \frac{\partial u_z}{\partial z} \right]^2. \quad (7)$$

It is seen that, for $(1 - \sigma^*)$ as large as 0.7, the total energy is still well conserved throughout the simulation, with the maximum deviation being less than 5%. Consequently, the present method is believed to be capable of accurately handling the problem concerned. It is also noted that the simulation of Blanchette *et al.* [16] shows about 10% variation of total energy at a surface tension difference of $(1 - \sigma^*) = 0.33$.

B. Effect of surface tension difference

To explore the underlying physics for the droplet ejection phenomena, we first simulated and compared the coalescence processes with different $(1 - \sigma^*)$, as shown in Fig. 5, in which case (a) is the benchmark case with uniform surface tension, and cases (b)–(d) have increasingly large surface

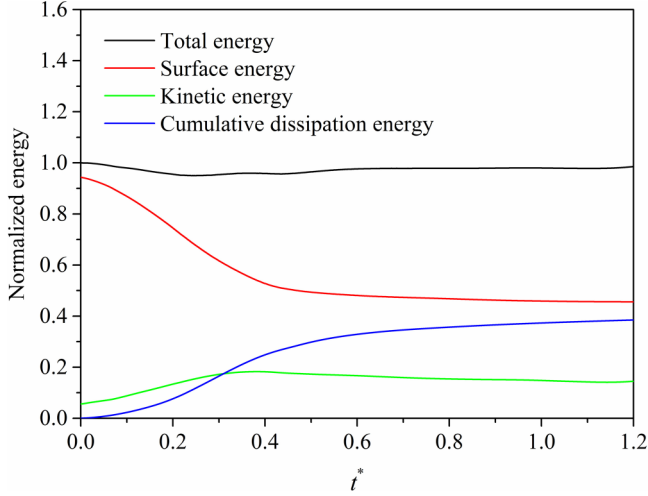


FIG. 4. Evolution of different energy components (normalized by the total energy) during the droplet coalescence shown in Fig. 3.

tension differences $(1 - \sigma^*)$. For all the cases, the Oh number and the We number are fixed at $Oh = 0.005$ and $We = 10^{-4}$, while $(1 - \sigma^*)$ is increased through reducing the surface tension of the reservoir. It is seen that, with the increase of the surface tension difference, the coalescence results in the non-monotonic outcome from “partial coalescence” to “total coalescence” and to “partial coalescence.”

In the benchmark case (a), the droplet tends to merge into the reservoir, driven by its capillary pressure, and it also experiences interfacial oscillation and results in partial coalescence finally. Following the initial contact of the droplet and the reservoir, a liquid bridge is built as illustrated in

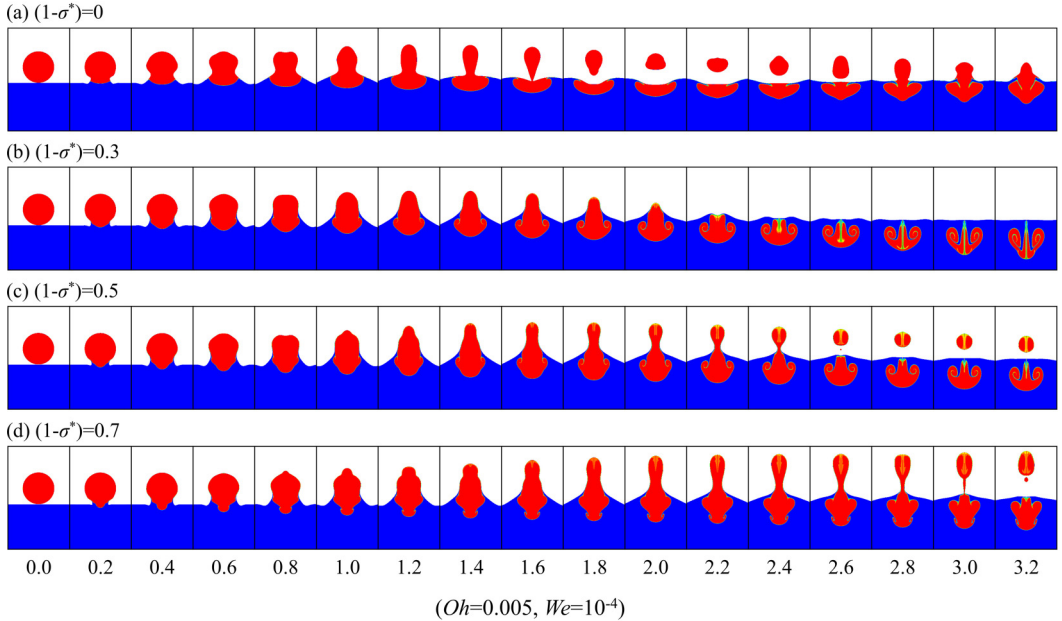


FIG. 5. Droplet coalescence at different surface tension differences (a) $(1 - \sigma^*) = 0$, (b) $(1 - \sigma^*) = 0.3$, (c) $(1 - \sigma^*) = 0.5$, (d) $(1 - \sigma^*) = 0.7$, and fixed $Oh = 0.005$ and $We = 10^{-4}$.

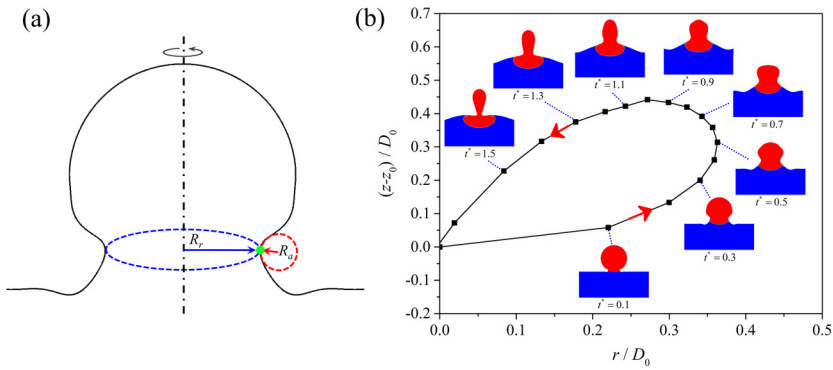


FIG. 6. Evolution of the liquid bridge of case (a) in Fig. 5. (a) Schematic of the liquid bridge, whose principal radii of curvature are denoted by R_a in the azimuthal direction and R_r in the radial direction. The representative point (green dot) on the bridge corresponds to the one closest to the axis. (b) Trajectory of the representative point, whose coordinates, (r, z) , with respect to the center of the initial liquid/air interface, $(0, z_0)$, are normalized by the droplet diameter D_0 .

Fig. 6(a), and the trajectory of the representative point with minimum distance to the axis is plotted in Fig. 6(b). It is seen that, the evolution of the liquid bridge mainly exhibits two stages. During the first stage, the liquid bridge expands horizontally outwards while rises up with the upwardly propagating capillary wave. During the second stage, the liquid bridge shrinks horizontally inwards with the downwardly retracting interface. Despite of its shift in the vertical position, the final breakup of the liquid bridge takes place close to the point of initial contact. Consequently, we can focus only on the horizontal motion of the liquid bridge, which is driven by the net capillary force $\Delta p = 2\sigma(R_a^{-1} - R_r^{-1})$, where R_a^{-1} and R_r^{-1} denote the azimuthal and the radial curvature of the bridge, respectively [see Fig. 6(a)]. Figure 7 compares two typical configurations of the liquid bridge during the initial expansion and the final shrinkage. It clearly shows that, compared to the initial expansion with $R_r^{-1} \ll R_a^{-1}$, R_a^{-1} is significantly reduced to $R_r^{-1} \gg R_a^{-1}$ during final shrinkage so that the strong horizontal inward capillary force squeezes the fluid away from the bridge and results in pinch-off. For simplicity and convenience of the following discussion, we follow the terminology of Blanchette

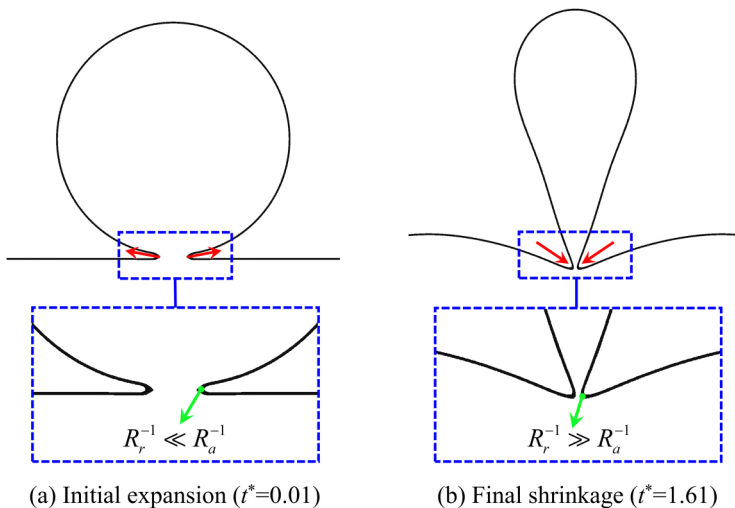


FIG. 7. Schematic of the liquid bridge during (a) the initial expansion and (b) the final shrinkage.

and Bigioni [9], who used “horizontal collapse” to denote the horizontal expansion and shrinkage of the bridge, and “vertical collapse” to denote the vertical retraction of the droplet as it merges with the interface. Therefore, partial coalescence occurs only when the vertical collapse sufficiently lags behind the horizontal collapse so that the liquid bridge has a small azimuthal curvature throughout its final shrinkage. In the present case, this is phenomenologically attributed to the propagation of the capillary wave on the droplet interface, which carries abundant liquid upwards and thereby retards the vertical collapse.

For a moderate surface tension difference $(1 - \sigma^*) = 0.3$, as shown in Fig. 5(b), partial coalescence cannot take place and the droplet merges completely with the reservoir. Driven by the Marangoni flow, the reservoir fluid climbs up the droplet, leading to a reduction of local surface tension on the droplet surface. As discussed above, the horizontal collapse is governed by the capillary force and therefore can be regarded as a large-wavelength and low-frequency oscillation of the interface, whose timescale can be estimated by $\sqrt{\rho_l R_0^3 / \sigma}$. Lowering the surface tension of the liquid bridge from σ_L to σ_S would result in a prolonged horizontal collapse since $\sqrt{\rho_l R_0^3 / \sigma_S} / \sqrt{\rho_l R_0^3 / \sigma_L} = \sqrt{1 / \sigma^*} > 1$. Therefore, partial coalescence no longer occurs when the vertical collapse becomes dominant over the horizontal collapse for $(1 - \sigma^*)$ exceeding a certain critical value. According to Ref. [16], the critical $(1 - \sigma^*)$ for the disappearance of partial coalescence is as small as 0.05 for a wide range of Oh numbers.

If the surface tension difference is further increased to $(1 - \sigma^*) = 0.5$, however, partial coalescence reappears as shown in Fig. 5(c). Compared with case (a), in which pinch-off occurs at $t^* \approx 1.63$, breakup of liquid bridge in case (c) takes a longer time of $t^* \approx 2.53$, and the ratio of the times is approximately $1.55 \approx \sqrt{1 / \sigma^*}$. This indicates that the breakup is also caused by the horizontal collapse, and that the reemergence of partial coalescence should be owing to the retarded vertical collapse. By further increasing the surface tension difference to $(1 - \sigma^*) = 0.7$, as shown in Fig. 5(d), partial coalescence still occurs in such an intense manner that the secondary droplet, after its detachment from the reservoir, keeps ascending rather than descending in Fig. 5(c). This implies that, although the horizontal collapse is postponed compared with that in case (c), the retardation of vertical collapse is more prominent than that of the horizontal collapse at sufficiently large surface tension differences.

To better understand the effect of Marangoni flow on the vertical collapse, which gives rise to the non-monotonic emergence of partial coalescence, the vertical trajectories of the droplet apex for various $(1 - \sigma^*)$ are compared in Fig. 8. To measure the Marangoni effect, the *Marangoni* number, generally defined by $\text{Ma} = \Delta\sigma L / (\mu_l D)$, where $\Delta\sigma = \sigma_L - \sigma_S$ is the surface tension difference, and L is the characteristic length [38], can be written as $\text{Ma} = (1 - \sigma^*) \text{Sc} / \text{Oh}^2$ if L takes D_0 , indicating that Marangoni flow intensifies with either increasing $(1 - \sigma^*)$ or decreasing the Oh number. As shown in the figure, during the initial coalescence ($t^* < 0.7$), the droplet apexes are not affected by the flow induced by the expansion of the liquid bridge, and their trajectories are independent of the Ma number. Subsequently, the droplet apex in case (a) is adequately lifted by the upward propagating capillary waves, but it in case (b) shows a suppressed lifting motion ($0.7 < t^* < 1.2$) before shrinking to the reservoir more rapidly, as the droplet interface covered by the lower surface tension fluid results in a weakened interfacial oscillation. In cases (c) and (d) with larger Ma numbers, the droplet apex exhibits otherwise enhanced upward movement and thereby significantly slows down the vertical collapse. Consequently, the reemergence of partial coalescence at larger surface tension differences should depend on whether the Marangoni flow is strong enough to generate a considerable lifting motion on the droplet apex to significantly retard the vertical collapse, otherwise the vertical collapse would be accelerated and total coalescence is thereby facilitated.

It should be also noted that, although molecular diffusion in the liquid-phase is slow, the mixing of the two liquids, as represented by the yellow/green regions in Fig. 5, shows an obvious enhancement for cases (b)–(d) compared to case (a), which was also observed in the simulation of the coalescence of either a droplet and a reservoir [16] or two droplets [39] with surface tension difference. Such enhanced mixing, as pointed out by Kim *et al.* [40,41], is caused by the significant vorticity generation from the propagating Marangoni flow, and the gradient in surface tension is therefore not limited to

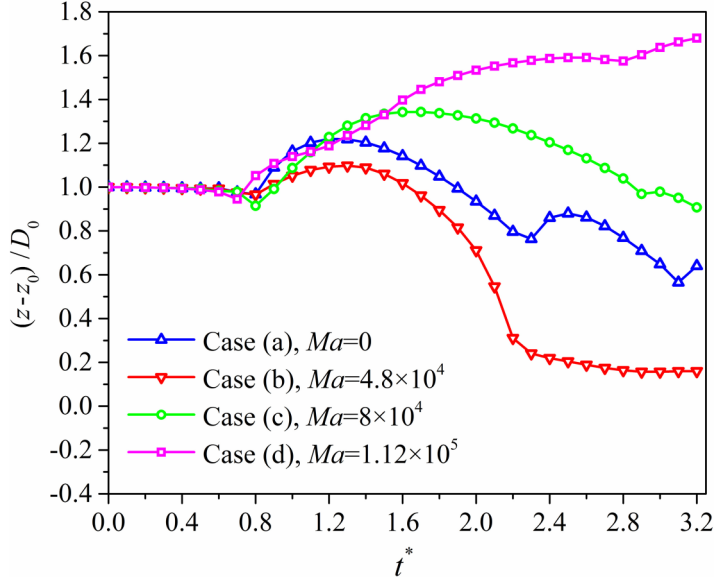


FIG. 8. Comparison of the vertical trajectory of the droplet apex for the cases in Fig. 5. z denotes the instantaneous vertical position of the droplet apex, and z_0 stands for the initial vertical coordinate of the interface. The difference in the Ma number is caused by $(1 - \sigma^*)$ since the Oh number is fixed.

the vicinity of the point where the two different fluids initially meet, but spans over a much larger length scale while the reservoir liquid spreading over the droplet surface.

C. Effect of viscous damping

Recognizing the critical role of Marangoni flow in facilitating partial coalescence, we shall further discuss the viscous effect since $Ma \propto Oh^{-2}$. Figure 9 shows the coalescence cases (a)–(d) corresponding to increasing Oh numbers, with fixed $(1 - \sigma^*) = 0.7$ and $We = 10^{-4}$. It is seen that the Marangoni flow is greatly damped by the viscous force with the increase of the Oh number, and that partial coalescence can occur when the Oh number is below a certain value, or the droplet will merge completely with the reservoir as shown in case (d). For cases (a)–(c) which result in partial coalescence, two different modes are further identified: (I) peak ejection at sufficiently small Oh number such as case (a), where the Marangoni flow is strong enough to entrain abundant fluids upwards and finally eject a secondary droplet from its peak; (II) bottom pinch-off at moderately small Oh numbers as cases (b) and (c), where the Marangoni flow is less intensive compared with that in case (a) but still able to lift the droplet to a certain height and facilitate pinch-off at the bottom bridge. It should be noted that Blanchette *et al.* discovered only peak injection in their limited experiments, where only two cases of droplet ejection are shown in Fig. 11(a) of Ref. [16].

It is noted that, the increase in the Oh number, apart from slowing down the Marangoni flow by the increased viscous force, may also dampens the horizontal collapse. As mentioned above, the horizontal collapse can be regarded as a large-wavelength, low-frequency oscillation of the interface, whose wavelength λ is on the order of R_0 . As such, the wavenumber and the angular frequency of the horizontal collapse could be estimated by $k_{\text{wave}} = 2\pi/\lambda \sim 2\pi/R_0$, and $\omega_0 \sim \sqrt{\sigma_S k_{\text{wave}}^3/\rho_l} = \sqrt{8\pi^3 \sigma_S/\rho_l R_0^3}$ [42], respectively. The effect of viscous damping on interfacial oscillation is considered

to be small as long as $k_{\text{wave}}/\sqrt{\omega_0 \rho_l/\mu_l} = (2\pi/R_0)/\sqrt{\sqrt{8\pi^3 \sigma_S/\rho_l R_0^3}/\mu_l} \approx 6.52Oh \ll 1$ [43], or equivalently $Oh \ll 0.15$, suggesting that the horizontal collapse of the cases in Fig. 9 with maximum $Oh = 0.015$ are not significantly affected by the viscous force. Therefore, the two modes of partial

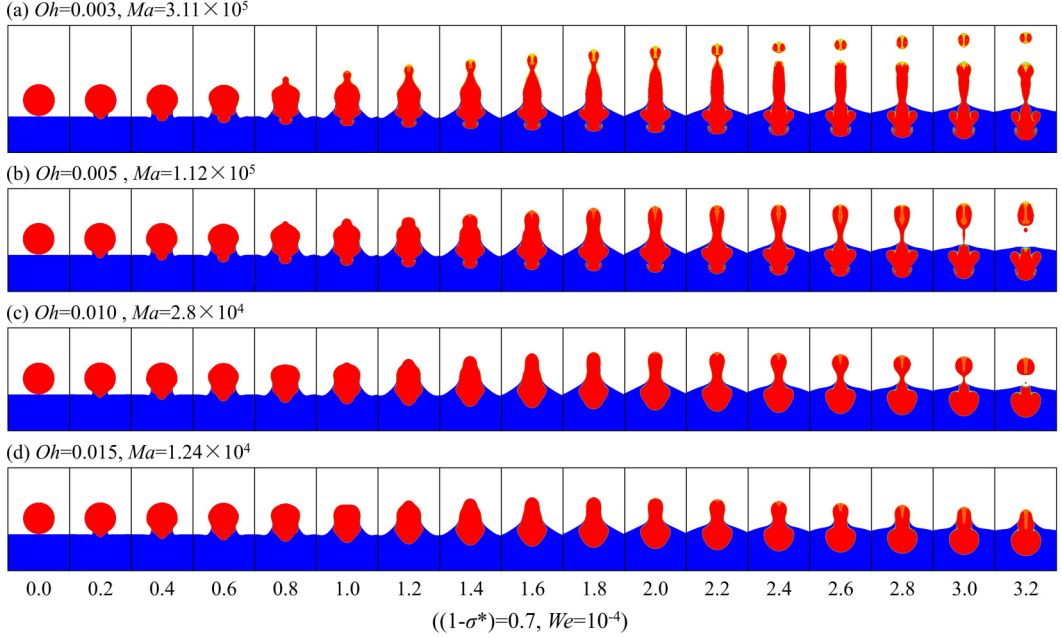


FIG. 9. Droplet coalescence at different Oh numbers (a) $Oh = 0.003$, (b) $Oh = 0.005$, (c) $Oh = 0.010$, (d) $Oh = 0.015$, and fixed $(1 - \sigma^*) = 0.7$ and $We = 10^{-4}$.

coalescence can be further explained by examining the dependence of the non-dimensional breakup time $t_{\text{break}}^* = t_{\text{break}} / \sqrt{\rho_l R_0^3 / \sigma_S}$ on the Oh number, in which t_{break} denotes the duration from the initial contact to the first breakup, and $\sqrt{\rho_l R_0^3 / \sigma_S}$ is the characteristic oscillation time of the lower surface tension interface. As shown in Fig. 10 for the cases with $Oh \leq 0.004$, peak ejection occurs and t_{break}^* decreases with decreasing Oh number. This indicates that the breakup shows no correlation with the interfacial oscillation and should be attributed to the Rayleigh-Plateau instability, since the

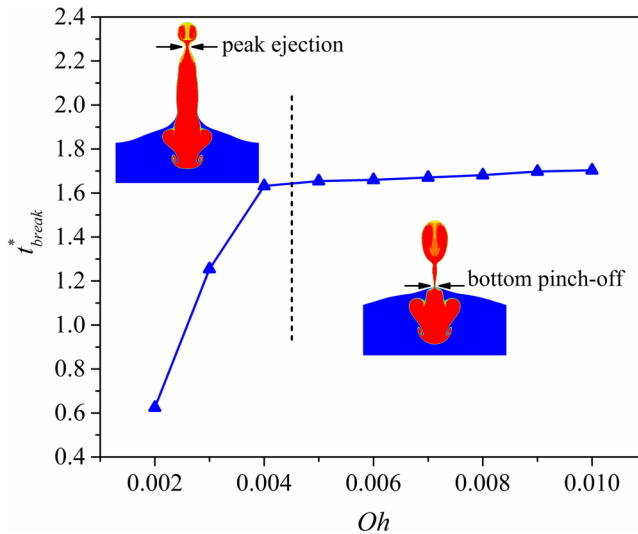


FIG. 10. Dependence of the normalized breakup time on the Oh number.

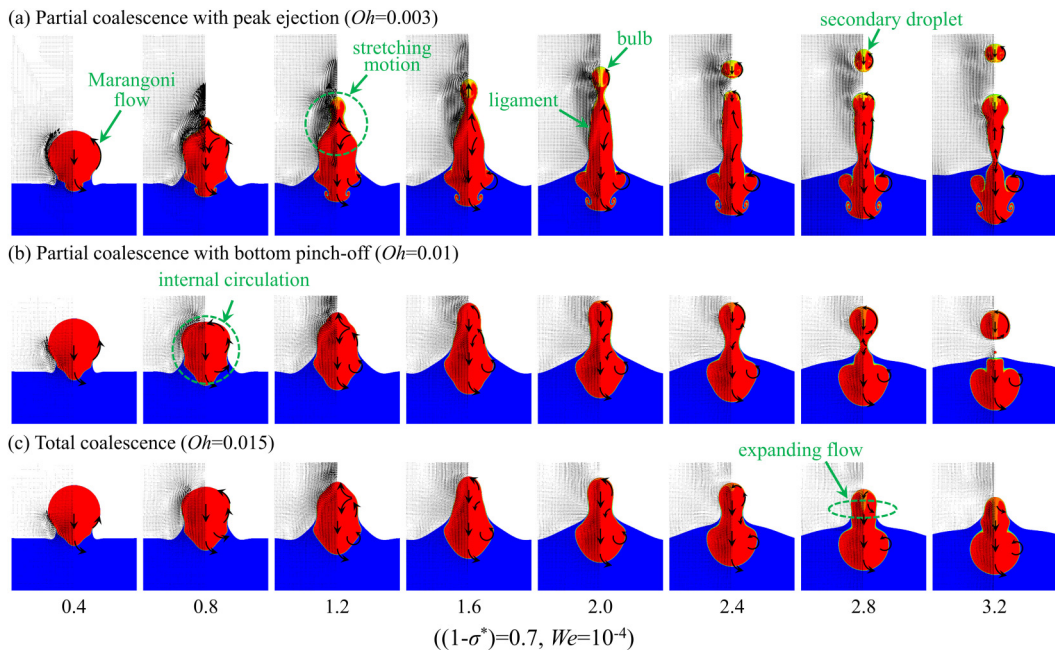


FIG. 11. Time evolution of the flow field for (a) partial coalescence with peak injection, (b) partial coalescence with bottom pinch-off, and (c) total coalescence at fixed $(1 - \sigma^*) = 0.7$ and $We = 10^{-4}$.

Marangoni flow is increasingly prominent in stretching the droplet into an elongated column shape with reduced viscous damping at lower Oh numbers. For the cases with $Oh > 0.004$, bottom pinch-off takes place and t_{break}^* levels off with increasing the Oh number, indicating that the breakup is caused by interfacial oscillation with the arrival of the horizontal collapse, which is not obviously affected by the viscous force.

The evolution of the flow fields in the typical cases of partial coalescence with peak injection, partial coalescence with bottom pinch-off, and total coalescence in Fig. 9, are sequentially drawn in Fig. 11. It is seen that, for the case (a) with the smallest Oh number, the Marangoni flow moves very fast on the droplet surface to the droplet apex, forming a strong converging flow towards the axis and stretching the droplet vertically into a column shape. The apex of the droplet, during the vertical elongation, keeps accumulating in the presence of downward capillary pressure gradient, and forms a bulb while the ligament below is still being stretched upwards. As the bulb grows, the neck finally breaks up as a result of Rayleigh-Plateau instability, and the secondary droplet continues ascending with its remaining inertia. In case (b) where bottom pinch-off occurs, the Marangoni flow is less intensive and the lifting motion is no longer observed for $t^* \geq 1.6$. It is also noted that, the Marangoni flow remains on the interface for a relatively long time after its initial convergence at the droplet apex, indicating that the propagating front of the lower surface tension fluid from the reservoir becomes diluted while wrapping up the droplet. This dilution could be ascribed to the enhance mixing due to Marangoni flow. For case (c), the Marangoni flow is even weaker and the lifting effect is hardly observed. Instead, the vertical collapse is accelerated rather than being prolonged in cases (a) and (b), and the liquid bridge transits from shrinking to expanding before it can generate a significant inward capillary force to facilitate pinch-off.

D. Critical condition for Marangoni-flow-induced partial coalescence

After clarifying the mechanisms of partial coalescence, we are now ready to address the question: under what condition does partial coalescence occur? Since the critical condition for the

disappearance of partial coalescence caused by the minor surface tension differences $[(1 - \sigma^*) < 0.1]$ has been clarified by Blanchette *et al.* [16], we only focus on the re-emergence of partial coalescence at sufficiently large $(1 - \sigma^*)$ in the present study. In view of the critical role of the Marangoni flow as discussed above, one may naturally presume that there is a critical Ma above which partial coalescence could take place. However, this assumption could be easily overthrown since Fig. 5(b) with $Ma = 4.8 \times 10^4$ results in total coalescence but Fig. 9(c) with much smaller $Ma = 2.8 \times 10^4$ results in partial coalescence.

Considering that the occurrence of partial coalescence depends on whether a remarkable lifting motion could be generated to retard the vertical collapse, we should pay attention to the competition between the downward flow driven by capillary pressure gradient and the upward fluid entrainment by Marangoni flow. Regarding to the scaling analysis, we followed the approach of Shim and Stone [18] to estimate the Marangoni flow velocity. Denote l to be the temporal distance that the lower-surface-tension fluid has propagated along the droplet surface, and the characteristic Marangoni flow velocity can therefore take $U_{Ma} = dl/dt$. Assume that the surface tension gradient is spread out over the length l , U_{Ma} is derived through balancing the Marangoni stress and the viscous stress as

$$U_{Ma} \sim (\delta/l)\Delta\sigma/\mu_l, \quad (8)$$

where δ denotes the interior fluid layer thickness entrained by the interfacial shear flow and is estimated by

$$\delta \sim \sqrt{\mu_l(l/U_{Ma})/\rho_l}. \quad (9)$$

Substituting Eq. (9) into Eq. (8) we have

$$U_{Ma} \sim [(\Delta\sigma)^2/(\rho_l\mu_l l)]^{1/3} = \alpha[(\Delta\sigma)^2/(\rho_l\mu_l l)]^{1/3}, \quad (10)$$

In which α is a proportionality constant. Note that $U_{Ma} = dl/dt$, $l(t)$ can be thereby obtained by solving Eq. (10) with the initial condition of $l(0) = 0$, which gives

$$l(t) = \theta[(\Delta\sigma)^2/(\rho_l\mu_l)]^{1/4}t^{3/4}, \quad (11)$$

in which $\theta = (4\alpha/3)^{3/4}$. Let $l(t) = \pi R_0$, the characteristic time for the Marangoni flow to reach the droplet apex is then given by

$$t_{up} = (\pi/\theta)^{4/3} [R_0^4 \rho_l \mu_l / (\Delta\sigma)^2]^{1/3}. \quad (12)$$

On the other hand, the downward acceleration of the droplet could be estimated by

$$du_z/dt = \nabla p/\rho_l \sim 2\sigma_L/(\rho_l R_0^2), \quad (13)$$

and the characteristic time for the droplet to fall over R_0 is given by

$$t_{down} = \sqrt{2R_0/(du/dt)} \sim \sqrt{\rho_l R_0^3/\sigma_L}. \quad (14)$$

By comparing these two time scales, we have

$$t_{down}/t_{up} = \sqrt{\rho_l R_0^3/\sigma_L} / [(\pi/\theta)^{4/3} [R_0^4 \rho_l \mu_l / (\Delta\sigma)^2]^{1/3}] \sim [(1 - \sigma^*)/\sqrt{Oh}]^{2/3}. \quad (15)$$

To generate a significant lifting motion, Marangoni flow should arrive at the droplet apex early enough before a considerable downward velocity is gained, suggesting that partial coalescence may occur when $(1 - \sigma^*)/\sqrt{Oh}$ exceeds a certain value. To verify this hypothesis, extensive simulations were conducted in the present study for a wide range of Oh numbers. As demonstrated in Fig. 12, a critical value of $(1 - \sigma^*)/\sqrt{Oh}$ does exist between partial and total coalescence and approximately equals to 6.75, which agrees well with the experiments by Blanchette *et al.* [16]. Physically, with the increase of the Oh number, larger surface tension difference is required to facilitate partial coalescence, while for water-ethanol-like systems with maximum $\sigma^* = 0.3$, Marangoni flow is not able to induce partial coalescence as long as $Oh > 0.01$.

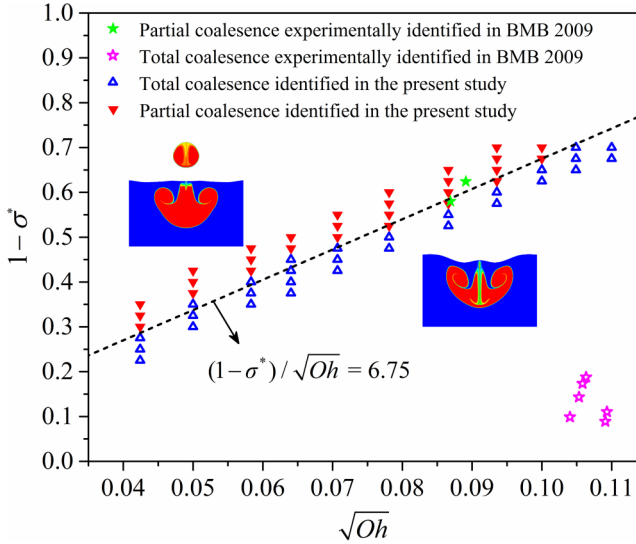


FIG. 12. Critical condition for Marangoni-flow-induced partial coalescence. BMB 2009 [16].

IV. CONCLUDING REMARKS

The coalescence of a droplet and a liquid/air interface of lower surface tension was numerically studied by using the phase-field method. The lattice Boltzmann method was employed as the computational platform for solving the flow field as well as the liquid/air interface. Both surface tension and Marangoni stress take the potential form in the simulation to relieve numerical difficulty in handling interfacial forces. To visualize internal mixing and capture the accompanied variation in surface tension, another transport equation for the fluid from the reservoir was also solved by using the finite difference method.

The simulation results show that, compared with the droplet coalescence of identical fluids, the surface tension difference causes an extra conversion of surface energy to kinetic energy through the Marangoni flow, and the coalescence results in a non-monotonic transition from “partial coalescence” to “total coalescence” and to “partial coalescence” with increasing surface tension difference. Such a non-monotonicity is caused by the competition between the horizontal and the vertical collapses. The horizontal collapse is governed by interfacial oscillation and prolongs monotonically with increasing surface tension difference. The vertical collapse is significantly affected by the Marangoni flow and behaves distinctly with different Ma numbers: if Ma is small, the upward lifting motion by the convergence of capillary wave would be weakened, since the droplet interface is covered by the lower surface tension fluid driven up by the Marangoni flow, and the vertical collapse is thereby accelerated; if Ma is large, the vertical collapse would be otherwise retarded by the upward fluid entrainment after the convergence of the Marangoni flow. Therefore, partial coalescence reemerges at sufficiently large surface tension difference as long as the retarded horizontal collapse overwhelms the even retarded vertical collapse.

The viscous force significantly dampens the propagation of the Marangoni flow, and the reemerged partial coalescence manifests two different modes such as peak injection and bottom pinch-off. Peak injection occurs in extremely low viscous situations and the secondary droplet is ejected from the peak owing to the Rayleigh-Plateau instability. Bottom pinch-off occurs in a range of higher Oh numbers and the breakup is owing to the interfacial oscillation.

Recognizing the decisive effect of the lifting motion of the droplet apex in facilitating partial coalescence, we derived the critical condition for the Marangoni-flow-induced partial coalescence by comparing the characteristic timescale of the upward Marangoni flow propagation with that of

the retraction driven by downward capillary pressure. Results show that partial coalescence occurs when $(1 - \sigma^*)/\sqrt{\text{Oh}}$ exceeds a certain value of approximately 6.75, which agrees well with the experimental observations by Blanchette *et al.* [16].

The present results apply to miscible fluids with differences in surface tension, which often emerges from the differences in either fluid temperature or fluid composition. The situation where surfactants induce the surface tension difference is similar to the present problem in that a Marangoni flow is also generated on the droplet surface. Differently, as the local concentration of the surfactants is affected by the expansion/contraction of the interface, the unevenly distributed surface tension during interfacial deformation would bring in additional interface elasticity that is not considered in the present study. Recent simulation by Martin and Blanchette [17] shows that, although the interface elasticity significantly affects the coalescence dynamics of a surfactant-laden liquid droplet on a surfactant-laden interface of the same liquid, the coalescence of a surfactant-free droplet (of a higher surface tension) with a surfactant-laden interface (of a lower surface tension) behaves similarly with one of the present simulations, where a moderate Marangoni effect would suppress partial coalescence. However, the re-emergence of partial coalescence at sufficiently large surface tension differences was not observed in their simulation. This is possibly because the limited range of parameters covered in their simulation result in $(1 - \sigma^*)/\sqrt{\text{Oh}} < 1.67$ ($(1 - \sigma^*) < 0.167$, $\text{Oh} > 0.01$ according to Fig. 9 in Ref. [17]), which is too small to cause partial coalescence, as the criteria determined by the present study is $(1 - \sigma^*)/\sqrt{\text{Oh}} > 6.75$.

ACKNOWLEDGMENTS

The work was financially supported by the National Natural Science Foundation of China (Grant No. 51606134) and the National Natural Science Funds for Distinguished Young Scholar (Grant No. 51525603). The work at the Hong Kong Polytechnic University was sponsored by the Hong Kong Research Grants Council/General Research Fund (Grants No. PolyU 152217/14E and No. PolyU 152651/16E).

-
- [1] F. Raes, R. V. Dingenen, E. Vignati, J. Wilson, J. Putaud, J. H. Seinfeld, and P. Adams, Formation and cycling of aerosols in the global troposphere, *Atmos. Environ.* **34**, 4215 (2000).
 - [2] V. E. Ziegler and B. A. Wolf, Bimodal drop size distributions during the early stages of shear induced coalescence, *Polymer* **46**, 9265 (2005).
 - [3] E. Villermaux, Fragmentation, *Annu. Rev. Fluid Mech.* **39**, 419 (2007).
 - [4] H. A. Stone, A. D. Stroock, and A. Ajdari, Engineering flows in small devices: Microfluidics toward a lab-on-a-chip, *Annu. Rev. Fluid Mech.* **36**, 381 (2004).
 - [5] D. Velev, B. G. Prevo, and K. H. Bhatt, On-chip manipulation of free droplets, *Nature* **426**, 515 (2003).
 - [6] S. T. Thoroddsen and K. Takehara, The coalescence cascade of a drop, *Phys. Fluids* **12**, 1265 (2000).
 - [7] G. E. Charles and S. G. Mason, The coalescence of liquid drops with flat liquid/liquid interfaces, *J. Colloid Sci.* **15**, 236 (1960).
 - [8] X. Chen, S. Mandre, and J. J. Feng, Partial coalescence between a drop and a liquid-liquid interface, *Phys. Fluids* **18**, 051705 (2006).
 - [9] F. Blanchette and T. Bigioni, Partial coalescence of drops at liquid interfaces, *Nat. Phys.* **2**, 254 (2006).
 - [10] B. Ray, G. Biswas, and A. Sharma, Generation of secondary droplets in coalescence of a drop at a liquid-liquid interface, *J. Fluid Mech.* **655**, 72 (2010).
 - [11] G. E. Charles and S. G. Mason, The mechanism of partial coalescence of liquid drops at liquid/liquid interfaces, *J. Colloid Sci.* **15**, 105 (1960).
 - [12] E. M. Honey and H. P. Kavehpour, Astonishing life of a coalescing drop on a free surface, *Phys. Rev. E* **73**, 027301 (2006).
 - [13] T. Gilet, K. Mulleners, J. P. Lecomte, N. Vandewalle, and S. Dorbolo, Critical parameters for the partial coalescence of a droplet, *Phys. Rev. E* **75**, 036303 (2007).

- [14] F. Blanchette and T. P. Bigioni, Dynamics of drop coalescence at fluid interfaces, *J. Fluid Mech.* **620**, 333 (2009).
- [15] F. H. Zhang, E. Q. Li, and S. T. Thoroddsen, Satellite Formation During Coalescence of Unequal Size Drops, *Phys. Rev. Lett.* **102**, 104502 (2009).
- [16] F. Blanchette, L. Messio, and J. W. M. Bush, The influence of surface tension gradients on drop coalescence, *Phys. Fluids* **21**, 072107 (2009).
- [17] D. W. Martin and F. Blanchette, Simulations of surfactant effects on the dynamics of coalescing drops and bubbles, *Phys. Fluids* **27**, 012103 (2015).
- [18] S. Shim and H. A. Stone, Damped coalescence cascade of liquid drops, *Phys. Rev. Fluids* **2**, 044001 (2017).
- [19] K. L. Pan and C. K. Law, Dynamics of droplet-film Collision, *J. Fluid Mech.* **587**, 1 (2007).
- [20] D. Jacqmin, Calculation of two-phase Navier–Stokes flows using phase-field modeling, *J. Comput. Phys.* **155**, 96 (1999).
- [21] P. Yue, J. J. Feng, C. Liu, and J. Shen, A diffuse-interface method for simulating two-phase flows of complex fluids, *J. Fluid Mech.* **515**, 293 (2004).
- [22] T. Lee and L. Liu, Lattice Boltzmann simulations of micron-scale drop impact on dry surfaces, *J. Comput. Phys.* **229**, 8045 (2010).
- [23] H. Liu, A. J. Valocchi, Y. Zhang, and Q. Kang, Lattice Boltzmann phase-field modeling of thermos capillary flows in a confined micro channel, *J. Comput. Phys.* **256**, 334 (2014).
- [24] R. Borcia and M. Bestehorn, Phase-field model for Marangoni convection in liquid-gas systems with a deformable interface, *Phys. Rev. E* **67**, 066307 (2003).
- [25] S. Chen and G. D. Doolen, Lattice Boltzmann method for fluid flows, *Annu. Rev. Fluid Mech.* **30**, 329 (1998).
- [26] R. Benzi, S. Succi, and M. Vergassola, The lattice Boltzmann equation: Theory and applications, *Phys. Rep.* **222**, 145 (1992).
- [27] T. Lee, Effects of incompressibility on the elimination of parasitic currents in the lattice Boltzmann equation method for binary fluids, *Comput. Math. Appl.* **58**, 987 (2009).
- [28] D. D’Humières, I. Ginzburg, M. Krafczyk, P. Lallemand, and L. Luo, Multiple-relaxation-time lattice Boltzmann models in three dimensions, *Phil. Trans. R. Soc. Lond. A* **360**, 437 (2002).
- [29] K. Sun, M. Jia, and T. Wang, Numerical investigation on the head-on collision between unequal-sized droplets with multiple-relaxation-time lattice Boltzmann model, *Int. J. Heat Mass Transf.* **70**, 629 (2014).
- [30] K. Sun, T. Wang, P. Zhang, and C. K. Law, Non-Newtonian flow effects on the coalescence and mixing of initially stationary droplets of shear-thinning fluids, *Phys. Rev. E* **91**, 023009 (2015).
- [31] K. Sun, P. Zhang, C. K. Law, and T. Wang, Collision Dynamics and Internal Mixing of Droplets of Non-Newtonian Liquids, *Phys. Rev. Appl.* **4**, 054013 (2015).
- [32] K. Sun, S. Yang, and C. K. Law, A diffuse interface method for simulating the dynamics of premixed flames, *Combust. Flame* **163**, 508 (2016).
- [33] S. Gottlieb and C. Shu, Total variation diminishing Runge-Kutta schemes, *Math. Comp.* **67**, 73 (1998).
- [34] G. Jiang and C. Shu, Efficient implementation of weighted ENO schemes, *J. Comput. Phys.* **126**, 202 (1996).
- [35] See Supplemental Material at <http://link.aps.org/supplemental/10.1103/PhysRevFluids.3.023602> for the effect of diffusion on the droplet coalescence process.
- [36] See Supplemental Material at <http://link.aps.org/supplemental/10.1103/PhysRevFluids.3.023602> for the grid-independence study.
- [37] See Supplemental Material at <http://link.aps.org/supplemental/10.1103/PhysRevFluids.3.023602> for the domain-width-independence study.
- [38] A. Thess, D. Sporn, and B. Jüttner, Viscous Flow at Infinite Marangoni Number, *Phys. Rev. Lett.* **75**, 4614 (1995).
- [39] F. Blanchette, Simulation of Mixing Within Drops Due to Surface Tension Variations, *Phys. Rev. Lett.* **105**, 074501 (2010).
- [40] H. Kim, J. Lee, T. H. Kim, and H. Y. Kim, Spontaneous marangoni mixing of miscible liquids at a liquid-liquid-air contact line, *Langmuir* **31**, 8726 (2015).

- [41] H. Kim, K. Muller, O. Shardt, S. Afkhami, and H. A. Stone, Solutal Marangoni flows of miscible liquids drive transport without surface contamination, [Nat. Phys. **13**, 1105 \(2017\)](#).
- [42] H. Lamb, *Hydrodynamics*, 6th ed. (Cambridge University Press, Cambridge, 1932).
- [43] F. Denner, Frequency dispersion of small-amplitude capillary waves in viscous fluids, [Phys. Rev. E **94**, 023110 \(2016\)](#).